J Mater Sci (2011) 46:2300–2307
DOI 10.1007/s10853-010-5073-4

Nanoscale fracture analysis by atomic force microscopy of EPDM rubber due to high-pressure hydrogen decompression

Junichiro Yamabe · Shin Nishimura

Received: 21 September 2010 / Accepted: 9 November 2010 / Published online: 30 November 2010

Abstract The relationship between internal fracture due to high-pressure hydrogen decompression and microstructure of ethylene–propylene–diene–methylene linkage (EPDM) rubber was investigated by atomic force microscopy (AFM). Nanoscale line-like structures were observed in an unexposed specimen, and their number and length increased with hydrogen exposure. This result implies that the structure of the unfilled EPDM rubber is inhomogeneous at a nanoscale level, and nanoscale fracture caused by the bubbles that are formed from dissolved hydrogen molecules after decompression occurs even though no cracks are observed by optical microscopy. Since this nanoscale fracture occurred at a threshold tearing energy lower than that obtained from static crack growth tests of macroscopic cracks ($T_{s,th}$), it is supposed that nanoscale structures that fractured at a lower threshold tearing energy ($T_{nano,th}$) than $T_{s,th}$ existed in the rubber matrix, and these low-strength structures were the origin of the nanoscale fracture. From these results, it is inferred that the fracture of the EPDM rubber by high-pressure hydrogen decompression consists of two fracture processes that differ in terms of size scale, i.e., bubble formation at a submicrometer level and crack initiation at a micrometer level. The hydrogen pressures at bubble formation and crack initiation were also estimated by assuming two threshold tearing energies, $T_{nano,th}$ for the bubble formation and $T_{s,th}$ for the crack initiation, in terms of fracture mechanics. As a result, the experimental hydrogen pressures were successfully estimated.

J. Yamabe (✉)
International Research Center for Hydrogen Energy,
Kyushu University, 744 Motooka, Nishi-ku,
Fukuoka 819-0395, Japan
e-mail: yamabe@mech.kyushu-u.ac.jp

S. Nishimura
Department of Mechanical Engineering, Kyushu University,
744 Motooka, Nishi-ku, Fukuoka 819-0395, Japan
e-mail: nishimura.shin.691@m.kyushu-u.ac.jp

J. Yamabe · S. Nishimura
Research Center for Hydrogen Industrial Use and Storage
(HYDROGENIUS), National Institute of Advanced Industrial
Science and Technology (AIST), 744 Motooka, Nishi-ku,
Fukuoka 819-0395, Japan

Introduction

In view of the depletion of fossil fuels and acceleration of global warming, there is growing international interest in hydrogen energy. To create a society based on hydrogen energy in the near future, it is necessary to clarify the influence of hydrogen on the mechanical, physical, and chemical properties of the materials used for hydrogen energy systems. In the case of rubber materials, there is a particular danger of mechanical damage due to internal fracture, which occurs when high-pressure hydrogen gas is suddenly decompressed. This internal fracture is sometimes referred to as blister fracture or explosive decompression failure (XDF) [1]. Although there are several reports on the internal fracture of rubber by high-pressure carbon dioxide, nitrogen, and argon gases [1–10], there are no reports on internal fracture by high-pressure hydrogen decompression.

In our previous studies [11–16], we clarified that internal fracture of rubber occurred by high-pressure hydrogen decompression. Furthermore, unfilled peroxide-crosslinked ethylene–propylene–diene–methylene linkage (EPDM) rubber, silica-filled peroxide-crosslinked EPDM rubber, and unfilled sulfur-vulcanized EPDM rubber were exposed to hydrogen gas at a maximum pressure of 10 MPa and the fracture surfaces obtained by decompression failure were

observed by scanning electron microscopy (SEM). As a result, we observed micrometer-size defects, silica agglomerates, and holes at the fracture origin, or we did not observe anything at the fracture origin. Figure 1 shows examples of SEM images of these fracture surfaces [13]. Figure 1a and b is SEM images of the unfilled peroxide-crosslinked EPDM rubber, while Fig. 1c and d is SEM images of the silica-filled peroxide-crosslinked EPDM rubber. The fractures shown in Fig. 1a and c originated from micrometer-size defects and silica agglomerates, respectively. In contrast, the fractures shown in Fig. 1b and d originated from sites without anything. Since the sites without anything became the origin of fractures similar to the sites with micrometer-size defects, silica agglomerates, and holes, their mechanical conditions at crack initiation can be considered to be equivalent.

Figure 2 shows a suggested fracture process of rubber materials by high-pressure hydrogen decompression based on the results obtained by optical microscopy (OM) and SEM [16]. This process suggests that submicrometer-size bubbles that are rarely observed by OM were formed at sites around micrometer-size defects and filler agglomerates (case I), or low-strength sites in relation to inhomogeneities of crosslink density (case III) after decompression, and then they grew with elapsed time; consequently, micrometer-size cracks were initiated due to the stress concentration of the developed bubbles. In the case of micrometer-size holes (case II), the holes were filled with hydrogen gas during hydrogen exposure, and cracks initiated from these holes after decompression. In the model shown in Fig. 2, the bubble is defined as a cavity with size ranging from submicrometer to micrometer and is composed of hydrogen gas that is rarely observed by OM. Since a rubber material often contains micrometer-size structural defects, it is considered that the bubbles hardly influence the macroscopic

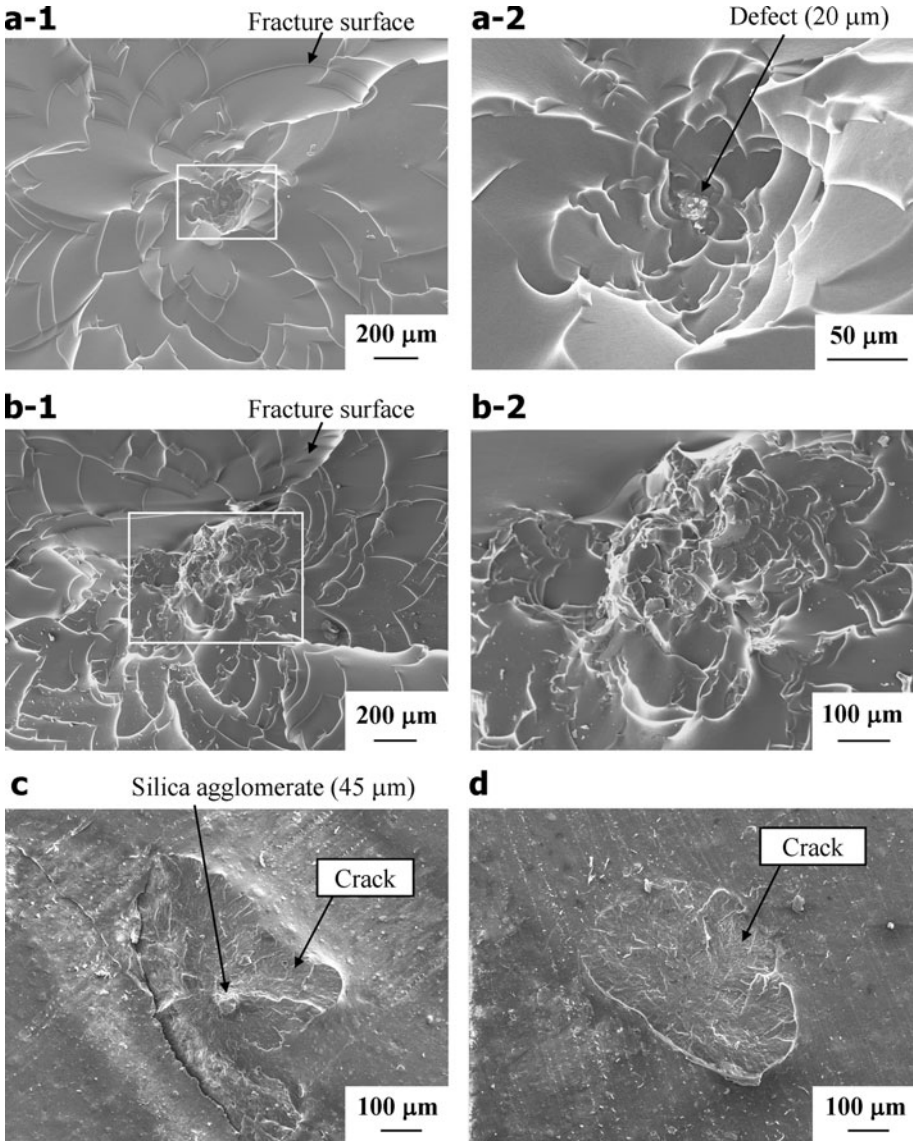

Fig. 1 Example of SEM images of fracture surfaces due to high-pressure hydrogen decompression: **a** fracture with micrometer-size defect of unfilled peroxide-crosslinked EPDM rubber, **a-1** low magnification, **a-2** high magnification; **b** fracture without anything of unfilled peroxide-crosslinked EPDM rubber, **b-1** low magnification, **b-2** high magnification; **c** fracture with silica agglomerate of silica-filled peroxide-crosslinked EPDM rubber; **d** fracture without anything of silica-filled peroxide-crosslinked EPDM rubber

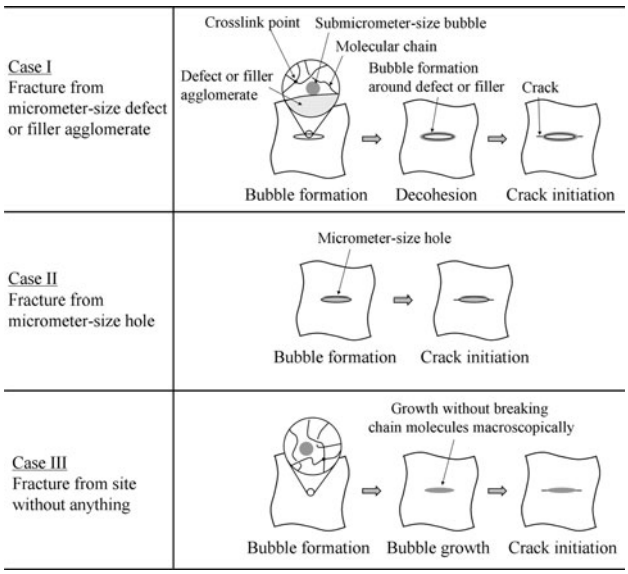

Fig. 2 Schematic representation of process of crack initiation

mechanical properties of the composite, such as elastic modulus and tensile strength, unless these bubbles grow and cause crack initiation. Therefore, the bubble can be regarded as a mechanically reversible cavity, while the crack is regarded as a mechanically irreversible cavity. Based on this suggested process, the hydrogen pressures at crack initiation (P_F) were estimated in terms of fracture mechanics [13, 14].

Table 1 shows the estimated hydrogen pressure at crack initiation of several EPDM rubbers. In the estimation, it was assumed that the crack was initiated when the tearing energy of a bubble (T) exceeded the threshold tearing energy of static crack growth ($T_{s,th}$) [17, 18]. When the bubble size was regarded as the maximum size of the defects, silica agglomerates, or holes observed by SEM, the estimated internal pressures at crack initiation (Π_F) were within the experimental hydrogen pressures at crack initiation (P_F). Therefore, when internal pressure (Π) can be regarded as being equal to hydrogen pressure (P), the hydrogen pressures at crack initiation of several EPDM rubbers were successfully estimated by this method, since $P_F \approx \Pi_F$. These previous studies successfully described the fracture process at a micrometer level. However, the process for case III in Fig. 2 was not clear, i.e., the process from bubble formation to crack initiation at a submicrometer level was not clear. In order to confirm the existence of submicrometer-size bubbles, the measurement of acoustic emission (AE) was also conducted.

Figure 3 shows the results of AE measurement of the hydrogen-exposed specimen made from unfilled peroxide-crosslinked EPDM rubber [16]. Tensile and static crack growth tests were conducted as preliminary tests; AE signals were measured during the fracture process in the static crack growth test, not during the deformation process in the tensile test. From the results of the hydrogen-exposed specimens, while no cracks were observed at 0.6 MPa (gage pressure), several cracks were observed at 5 and 10 MPa by OM. Then, the AE event count and amplitude increased when the number and size of the cracks increased with an increase in hydrogen pressure. Furthermore,

Table 1 Estimation of hydrogen pressure at crack initiation of several EPDM rubbers

Materials	p_F (MPa)	Bubble size (μm)	$T_{s,th}$ (N/m)	Π_F (MPa)
Unfilled peoxide-crosslinked	1.0–1.5	20	50	1.137
Unfilled sulfur-vulcanized	1.5–2.0	20	100	1.551
Silica-filled peoxide-crosslinked	4.0–4.5	45	220	4.287

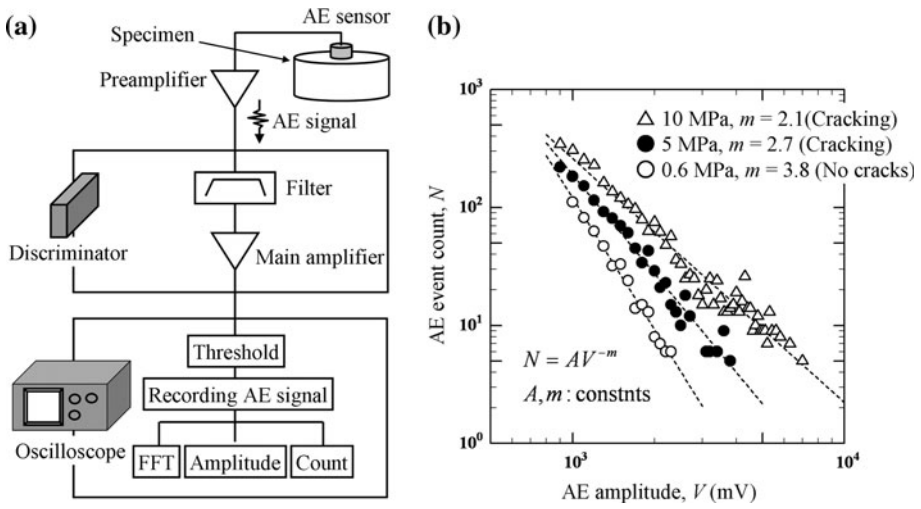

Fig. 3 Measurement of acoustic emission of hydrogen-exposed specimen made from unfilled peroxide-crosslinked EPDM rubber: **a** schematic representation of AE measurement, **b** relationship between AE event count and amplitude

although no cracks were observed by OM, AE signals were detected from the specimen exposed to hydrogen gas at 0.6 MPa. This result indicates that small-scale (nanoscale) fracture occurs by high-pressure hydrogen decompression, even though no cracks are observed by OM. This nanoscale fracture is considered to be due to bubble formation. From the results of AE, although we can indirectly confirm the nanoscale fracture, we have not yet obtained direct evidence of this fracture.

The objective of this study was to clarify the relationship between the nanoscale fracture process and the microstructure of rubber. For this reason, an unfilled EPDM rubber was employed, and then the microstructure of unexposed and hydrogen-exposed specimens was observed by atomic force microscopy (AFM). Furthermore, it was proposed that the multi-scale fracture process of the EPDM rubber was due to high-pressure hydrogen decompression, and the hydrogen pressures at bubble formation and crack initiation were estimated in terms of fracture mechanics.

Experimental

Material

We utilized unfilled peroxide-crosslinked EPDM rubber, which was a compound of EPDM, dicumyl peroxide with 1.6 phr (parts by weight per hundred parts of rubber), and stearic acid with 0.5 phr. Since this material is transparent, it is possible to observe crack initiation and growth behavior in the specimen by using OM. Density and durometer hardness (Type A) were 0.873 g/cm^3 and 51, respectively. This material is the same as that used for AE measurement in the previous study [15].

Specimen and experimental method

A cylindrical specimen with diameter of 29.0 mm and thickness of 12.5 mm made from the EPDM rubber was exposed to hydrogen gas at a maximum pressure of 10 MPa, 30 °C for 24 h by using a high-pressure hydrogen vessel (Fig. 4a). The cylindrical specimen was taken from the hydrogen vessel after hydrogen exposure (Fig. 4b), and crack initiation behavior was observed by OM (Keyence, VHX-900). After retained hydrogen molecules were perfectly diffused from the specimen, the specimen was cut with a cutter (Fig. 4c); the surface where no cracks were observed by OM was finished by a cryomicrotome (Leica Microsystems, EM FC6) as shown in Fig. 4d.

The finished surface was observed by AFM (Veeco, Dimension 3100/Nanoscope V). The spring constant of the cantilever was 40 N/m, the tip radius was less than 10 nm, and the resonance frequency was 300 kHz. Measurement was conducted in intermittent contact mode under atmospheric pressure at room temperature (20–25 °C).

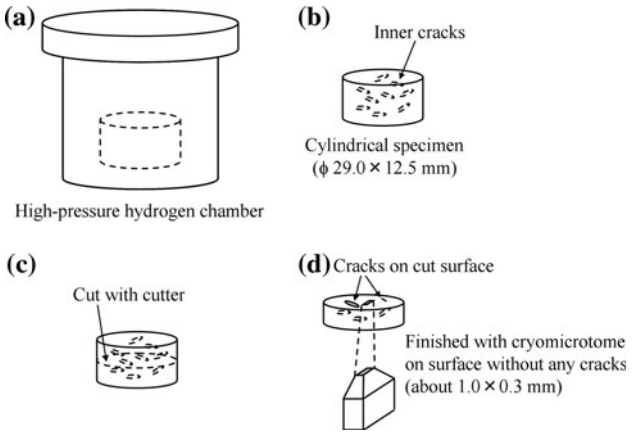

Fig. 4 Preparation of specimen for measurement by atomic force microscopy (AFM): **a** hydrogen exposure, **b** observation of crack initiation and growth after decompression, **c** cutting with cutter, **d** finishing with cryomicrotome

Results and discussion

Behavior of crack initiation

Figure 5 shows the crack initiation behavior of hydrogen-exposed specimens obtained by OM. The cracks were observed in the specimen exposed to hydrogen gas at 2 MPa or more, and the number and size of cracks increased with the increase in hydrogen pressure. The hydrogen pressure at crack initiation (P_F) ranged from 1.5 to 2 MPa. Although no cracks were observed in the specimen exposed to hydrogen gas at 0.6 MPa as shown in Fig. 5b, AE signals generated by the fracture process were detected from this hydrogen-exposed specimen in the previous study [16].

Observation of microstructure by AFM

Figure 6 shows height and amplitude-error images of unexposed and hydrogen-exposed (10 MPa) specimens. From Fig. 6a-1 and b-1, line-like structures about 100 nm in length can be seen in the unexposed specimen, although we cannot see any cracks and structures by OM. Figure 6a-2 and b-2 shows height and amplitude-error images of the specimen exposed to hydrogen at 10 MPa. The number and length of line-like structures increased with hydrogen exposure.

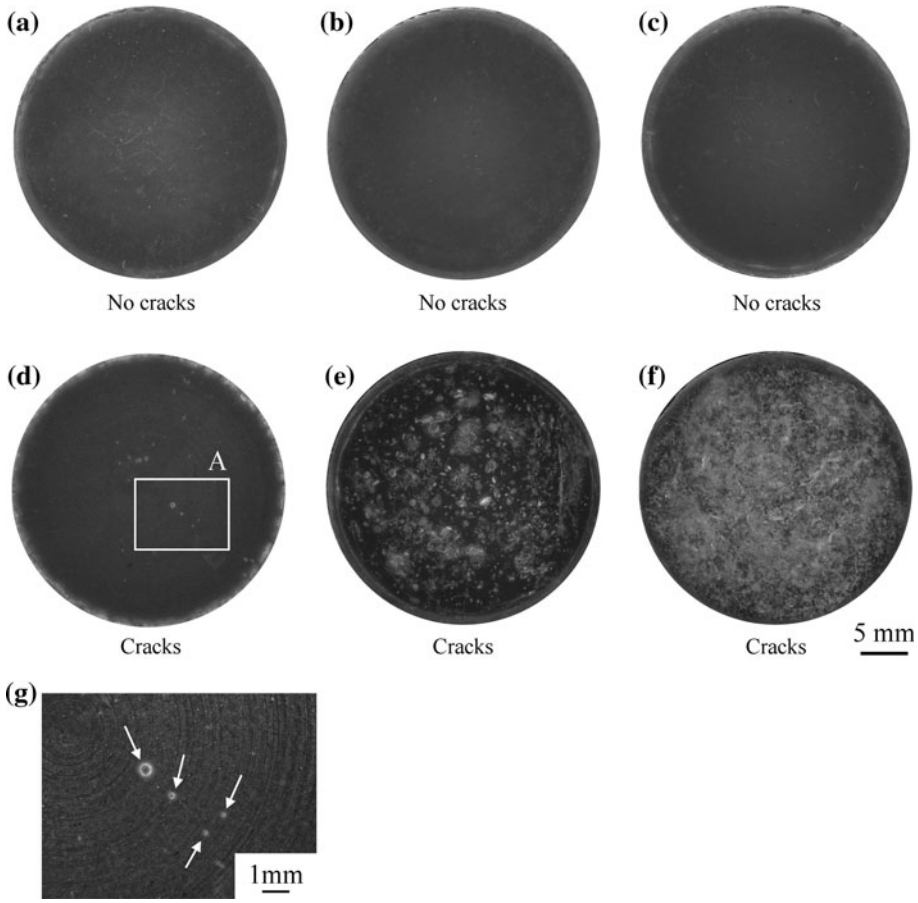

Fig. 5 Crack initiation condition due to high-pressure hydrogen decompression by optical microscopy: **a** unexposed, **b** 0.6 MPa, **c** 1.5 MPa, **d** 2 MPa, **e** 5 MPa, **f** 10 MPa, **g** magnification image of A

Figure 7 shows a three-dimensional height image of the specimen exposed to hydrogen at 10 MPa. Figure 8 shows a line profile of cross-section a–a′ shown in Fig. 7a. The line-like structures were dented, and the width of the line-like structure in cross-section a–a′ was 15 nm, and the depth was 2.8 nm. Since the number and size of the line-like structures depend on the observation area, 10 areas were observed by AFM.

Figure 9 shows a histogram of the number of line-like structures observed in the unexposed and hydrogen-exposed (10 MPa) specimens. The number of line-like structures per observation area (2×2 μm) in the unexposed specimen ranged from 5 to 25 (average 10), while that in the hydrogen-exposed (10 MPa) specimen ranged from 15 to 45 (average 32). Table 2 shows the average number, length, width, and depth of line-like structures of the unexposed and hydrogen-exposed (10 MPa) specimens. The average number and length of line-like structures increased with hydrogen exposure, while the average width and depth was hardly influenced by hydrogen exposure. The increase in number and length of line-like structures with hydrogen exposure is considered to be due to nanoscale fracture by bubbles formed from dissolved hydrogen molecules after decompression.

Process of nanoscale fracture

It is believed that submicrometer-size bubbles that are rarely observed by OM were formed after decompression and subsequently caused nanoscale fracture. According to fracture mechanics, nanoscale fracture occurs when the tearing energy of bubbles (T) exceeds the fracture energy (Γ_F). If Γ_F is assumed to be equal to the threshold tearing energy of static crack growth of macroscopic cracks ($T_{s,th}$), it would be impossible for the nanoscale fracture to occur, since these submicrometer-size bubbles need high internal pressure for their formation. However, the rubber structure is not homogeneous but inhomogeneous as seen in Fig. 6. The inhomogeneity of rubber structures has been reported in several papers [19, 20]. Therefore, it is considered that inhomogeneous structures with a lower threshold tearing energy than $T_{s,th}$ exist in the rubber matrix, and the nanoscale fracture occurs in these low-strength structures. The low-strength structures are assumed to be formed in relation to the inhomogeneity of crosslink density.

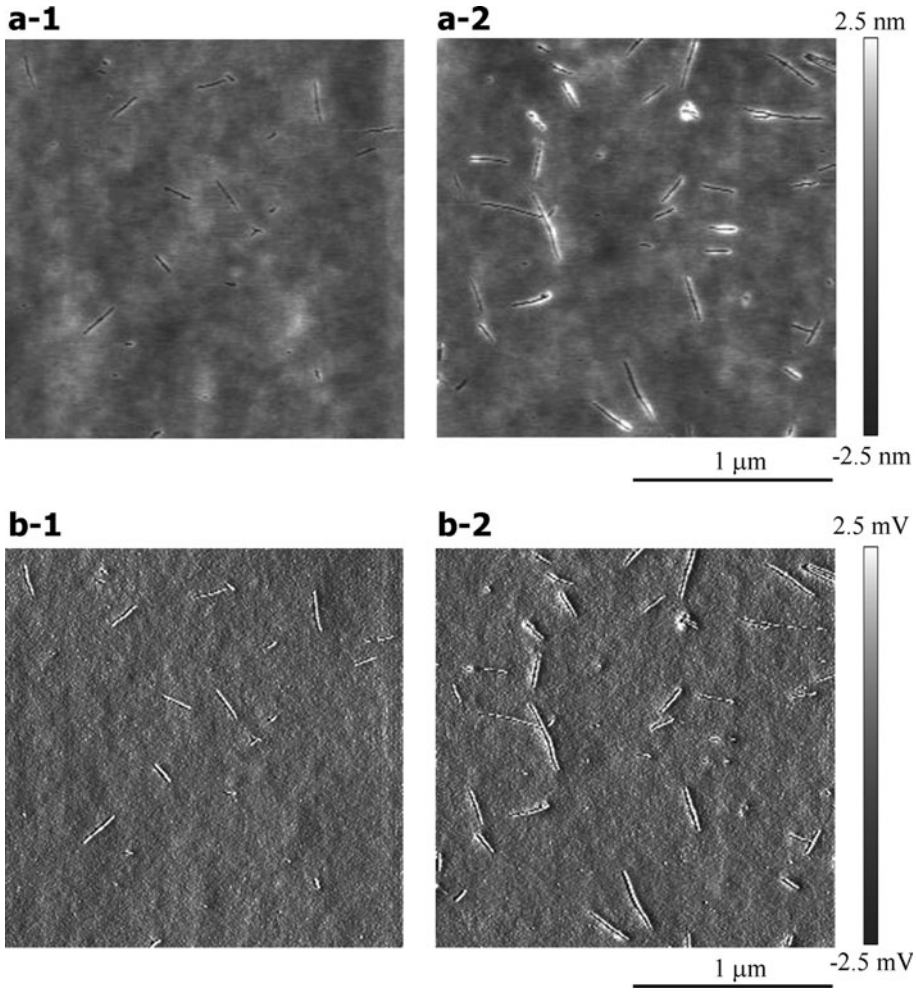

Fig. 6 Height and amplitude-error images of unexposed and 10 MPa hydrogen-exposed specimens by AFM: **a** height image, **a-1** unexposed specimen, **a-2** 10 MPa hydrogen-exposed specimen; **b** amplitude-error image, **b-1** unexposed specimen, **b-2** 10 MPa hydrogen-exposed specimen

Estimation of hydrogen pressure at bubble formation and crack initiation

Whether or not a crack is initiated is decided by the condition where the tearing energy of bubbles exceeds the threshold tearing energy of a static crack ($T_{s,th}$). In the previous studies [11–16], the bubble was regarded as a disc-like cavity, and its tearing energy was calculated by the finite element method (FEM). As a result, the hydrogen pressures at crack initiation of several EPDM rubbers were successfully estimated under the condition that $T \geq T_{s,th}$ ($=\Gamma_F$) as shown in Table 1. The hydrogen pressure at crack initiation (P_F) of the EPDM rubber used in this study was also evaluated in the previous study [16]. When the threshold tearing energy was 55 N/m, and the bubble size at crack initiation was assumed to be 14 μm, which was the maximum defect size observed on the fracture surfaces, the hydrogen pressure at crack initiation was estimated to be 1.53 MPa. Since the experimental hydrogen pressure at crack initiation ranged from 1.5 to 2.0 MPa, the P_F value was successfully estimated, as shown in Table 3.

In contrast, it is estimated that the hydrogen pressure at nanoscale fracture due to bubble formation ranged from 0.5 to 0.6 MPa by the measurement of AE, since AE signals generated by the fracture process were detected at 0.6 MPa or more and were not detected at 0.5 MPa or less [16]. It is supposed that the nanoscale fracture originates from low-strength structures with a lower threshold tearing energy than $T_{s,th}$; therefore, the Γ_F value of the low-strength structures was assumed to be equivalent to the surface energy when bubbles are formed in simple liquids (50×10^{-3}N/m) [2] in this study. Under this assumption, the hydrogen pressure at nanoscale fracture is estimated to be 0.57 MPa when the bubble size is 300 nm, which is the maximum length of the line-like structures observed in the unexposed specimen, as shown in Table 3. Since the estimated hydrogen pressure at nanoscale fracture was within the experimental result, the hydrogen pressure at nanoscale fracture was also successfully estimated as well as that at crack initiation in terms of fracture mechanics. These results imply that nanoscale low-strength structures with considerably lower threshold tearing energy than that

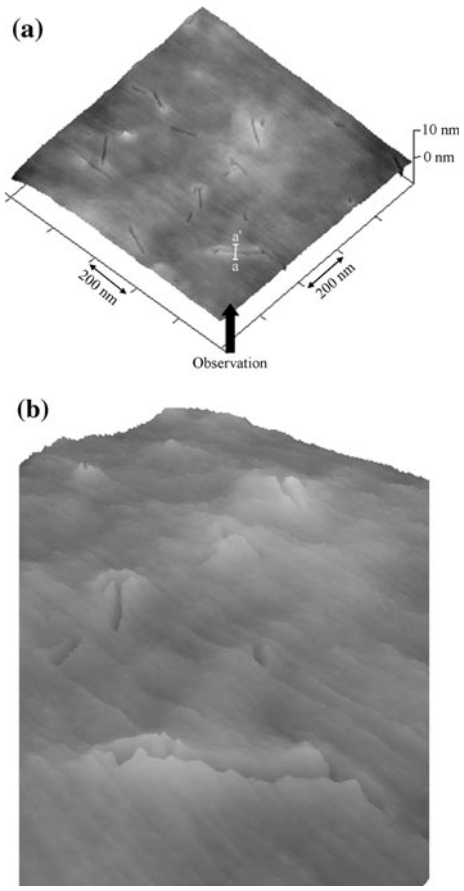

Fig. 7 Height image of 10 MPa hydrogen-exposed specimen: **a** three-dimensional image, **b** magnification image

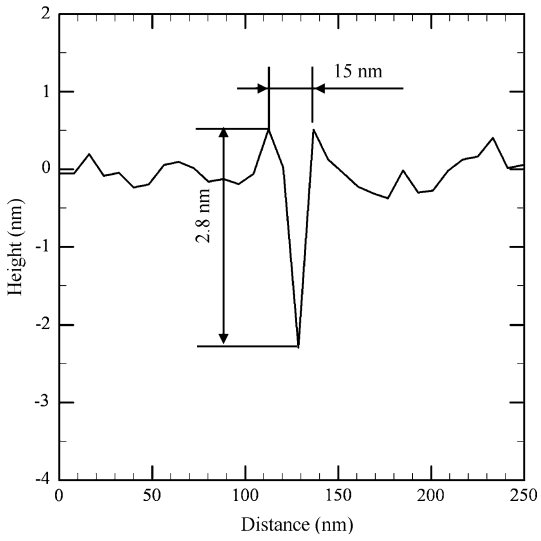

Fig. 8 Line profile of line-like structure

obtained from a static crack growth test of macroscopic cracks exist in the rubber structure; then, submicrometer-size bubbles originate from these low-strength structures prior to crack initiation. It is believed that some of these

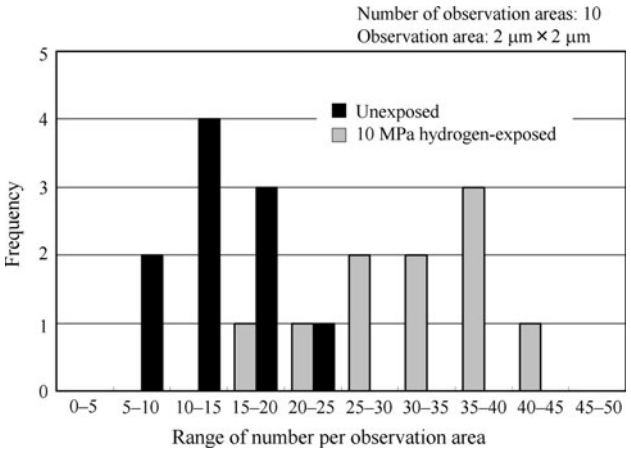

Fig. 9 Histogram of number of line-like structures observed in unexposed and 10 MPa hydrogen-exposed specimens

submicrometer-size bubbles grow and eventually cause crack initiation. The fracture surface shown in Fig. 1c is considered to be the result of this process.

Conclusions

In order to clarify the relationship between the nanoscale fracture process and the microstructure of an unfilled peroxide-crosslinked EPDM rubber, the microstructure of unexposed and hydrogen-exposed specimens was observed by AFM. The results obtained can be summarized as follows:

1. Nanoscale line-like structures were observed in an unexposed specimen, and the number and length of line-like structures increased with hydrogen exposure. The increase is considered to be due to nanoscale fracture by bubbles formed from dissolved hydrogen molecules after decompression.
2. According to fracture mechanics, nanoscale fracture occurs when the tearing energy of bubbles (T) exceeds the fracture energy (Γ_F). If Γ_F is assumed to be equal to the threshold tearing energy obtained from a static crack growth test of macroscopic cracks ($T_{s,th}$), it would be impossible for the nanoscale fracture to occur, since these nanoscale bubbles need high internal pressure for their formation. Therefore, it was inferred that nanoscale inhomogeneous structures with lower threshold tearing energy than $T_{s,th}$ existed in the rubber matrix, and the nanoscale fracture originated in these low-strength structures.
3. The hydrogen pressures at bubble formation and crack initiation were estimated under the assumption that crack initiation occurs when the tearing energy of bubbles (T) exceeds the threshold tearing energy

Table 2 Average number, length, width, and depth of the line-like structures of unfilled and 10 MPa hydrogen-exposed specimens by AFM

Materials	Average number per observed area (2 μm × 2 μm)	Average length (nm)	Average width (nm)	Average depth (nm)
Unexposed	10	102	15	4.3
10 MPa hydrogen-exposed	32	268	16	3.6

Table 3 Estimation of hydrogen pressures at bubble formation and crack initiation

Items	Experiment (MPa)[a]	Method	Energy (N/m)	Size (μm)	Estimation (MPa)[a]
Bubble formation (Nanoscale fracture)	0.5–0.6	Acoustic emission	50×10^{-3}	0.3	0.57
Crack initiation (Microscale fracture)	1.5–2.0	Optical microscope	55[b]	14	1.53

[a] Gage pressure (=absolute pressure − 0.1 MPa)

[b] This value was obtained from static crack growth tests

of static cracks ($T_{s,th}$), while bubble formation occurs when the tearing energy of the bubbles exceeds the nanoscopic threshold tearing energy ($T_{nano,th}$), which is considerably lower than $T_{s,th}$. The experimentally obtained $T_{s,th}$ value was 55 N/m, and the $T_{nano,th}$ value was assumed to be equivalent to the surface energy when bubbles are formed in simple liquids (50×10^{-3}N/m). As a result, the experimental hydrogen pressures at bubble formation and crack initiation were successfully estimated. The results imply that the fracture of the EPDM rubber by high-pressure hydrogen decompression consists of two fracture processes that differ in terms of size scale, i.e., bubble formation at a submicrometer level and crack initiation at a micrometer level.

Acknowledgement This research was supported by the NEDO Fundamental Research Project on Advanced Hydrogen Science (2006–2012).

References

1. Briscoe BJ, Savvas T, Kelly CT (1994) Rubber Chem Technol 67:384
2. Gent AN, Tompkins DA (1969) J Appl Phys 40:2520
3. Gent AN, Lindley PB (1958) Proc R Soc Lond A 249:195
4. Lindsey CH (1967) J Appl Phys 38:4843
5. Stevenson A, Glyn M (1995) Rubber Chem Technol 68:197
6. Stewart CW (1970) J Polym Sci A 8:937
7. Zakaria S, Briscoe BJ (1990) Chemtech 20:492
8. Ender DH (1986) Chemtech 16:52
9. Briscoe BJ, Liatsis D (1992) Rubber Chem Technol 65:350
10. Epstein PS, Plesset MS (1950) J Chem Phys 18:1505
11. Yamabe J, Nishimura S (2009) Trans J Soc Mech Eng A 75:633
12. Yamabe J, Nishimura S (2009) Trans J Soc Mech Eng A 75:1726
13. Yamabe J, Nishimura S (2010) In: 18th European conference on fracture, CD-ROM
14. Yamabe J, Nishimura S (2009) In: Proceedings of the 14th symposium on fracture and fracture mechanics, pp 30–34
15. Yamabe J, Nishimura S (2009) Int J Hydrogen Energy 34:1977
16. Yamabe J, Matsumoto T, Nishimura S (2010) J Soc Mater Sci Jpn 59:956
17. Thomas AG (1960) J Appl Polym Sci 8:168
18. Lake AJ, Lindley PB (1964) J Appl Polym Sci 8:707
19. Ikeda Y, Yasuda Y, Hijikata K, Tosaka M, Kohjiya S (2008) Macromolecules 41:5876
20. Dohi H, Sakai M, Nakamae H, Kimura H, Kotani M, Kishimoto H, Minagala Y (2007) Kautsch Gummi Kunstst 01–02:52